Chemistry & Biology
Article

Directed Evolution and Structural Characterization of a Simvastatin Synthase

Xue Gao,[1,3] Xinkai Xie,[1,3] Inna Pashkov,[2] Michael R. Sawaya,[2] Janel Laidman,[2] Wenjun Zhang,[1] Ralph Cacho,[2] Todd O. Yeates,[2,*] and Yi Tang[1,*]
[1]Department of Chemical and Biomolecular Engineering
[2]Department of Chemistry and Biochemistry
University of California, Los Angeles, Los Angeles, CA 90095, USA
[3]These authors contributed equally to this work
*Correspondence: yitang@ucla.edu (Y.T.), yeates@mbi.ucla.edu (T.O.Y.)
DOI 10.1016/j.chembiol.2009.09.017

SUMMARY

Enzymes from natural product biosynthetic pathways are attractive candidates for creating tailored biocatalysts to produce semisynthetic pharmaceutical compounds. LovD is an acyltransferase that converts the inactive monacolin J acid (MJA) into the cholesterol-lowering lovastatin. LovD can also synthesize the blockbuster drug simvastatin using MJA and a synthetic α-dimethylbutyryl thioester, albeit with suboptimal properties as a biocatalyst. Here we used directed evolution to improve the properties of LovD toward semisynthesis of simvastatin. Mutants with improved catalytic efficiency, solubility, and thermal stability were obtained, with the best mutant displaying an ~11-fold increase in an *Escherichia coli*-based biocatalytic platform. To understand the structural basis of LovD enzymology, seven X-ray crystal structures were determined, including the parent LovD, an improved mutant G5, and G5 cocrystallized with ligands. Comparisons between the structures reveal that beneficial mutations stabilize the structure of G5 in a more compact conformation that is favorable for catalysis.

INTRODUCTION

Tailoring enzymes found in natural product biosynthetic pathways catalyze a wide array of reactions, including acyltransfer (Loncaric et al., 2006), glycosylation (Zhang et al., 2006), hydroxylation (Rix et al., 2002), and halogenation (Neumann et al., 2008). A number of these enzymes decorate biologically inactive precursors into pharmaceutically active molecules via regioselective and stereoselective transformations. As a result, tailoring enzymes are attractive candidates as biocatalysts toward synthesis of semisynthetic derivatives and drug libraries (Zhou et al., 2008). LovD is an acyltransferase found in *Aspergillus terreus* and is responsible for converting the inactive precursor monacolin J acid (MJA) into the cholesterol-lowering drug lovastatin (LV, acid form lovastatin acid: LVA) via acylation of the α-*S*-methylbutyrate side chain (Kennedy et al., 1999; Xie et al., 2006) (Figure 1). The importance of the hydrophobic α-*S*-methylbutyryl side chain for binding of LVA to HMG-CoA reductase has been structurally confirmed (Istvan and Deisenhofer, 2001). Chemical modification of the LV side chain to α-dimethylbutyrate yielded the semisynthetic derivative simvastatin (SV, acid form simvastatin acid: SVA), which is the active pharmaceutical ingredient in the blockbuster drug Zocor® (Hoffman et al., 1986). Semisynthesis of SV from LV is a multiple-step chemical process and is therefore an intensely pursued target for devising an efficient biocatalytic approach (Berg et al., 2009; Morgan et al., 2006). As a result, LovD is a prime candidate to serve as such a biocatalyst.

LovD is a 413 amino acid protein predicted to have an α/β hydrolase fold based on primary sequence analysis (Kennedy et al., 1999). Among enzymes of known structure that are homologous to LovD is cephalosporin esterase, EstB (PDB ID 1CI9, 26% sequence identity) from *Burkholderia gladioli* (Wagner et al., 2002). The likely general base Tyr188, as well as a conserved SXXK patch that contains the active site nucleophile Ser76, were indicated through alignment of LovD with EstB (Figure 2A) (Petersen et al., 2001). During LVA biosynthesis, the α-*S*-methylbutyrate side chain is synthesized by the lovastatin diketide synthase (LDKS) LovF, and is then transferred by LovD regioselectively to the C8 hydroxyl of MJA via an unprecedented polyketide offloading mechanism (Xie et al., 2009a). The protein-protein interaction between LovD and the acyl carrier protein (ACP) domain of LovF facilitates this highly efficient tailoring reaction in *A. terreus*. We have previously explored the substrate promiscuity of LovD and have shown that it can also synthesize SVA by using the small molecule substrate α-dimethylbutyryl-*S*-methyl-mercaptoproprionate (DMB-SMMP) as an acyl donor (Xie and Tang, 2007) (Figure 1). Using *Escherichia coli* as an expression host, a whole-cell biocatalytic platform for converting MJA to SVA was established that can produce SVA with low throughput (Xie and Tang, 2007). However, as with many enzymes that have been removed from their natural context, LovD is catalytically suboptimal as a biocatalyst and suffers from poor thermal stability (Arnold, 2001). The catalytic activity of SVA synthesis using DMB-SMMP is attenuated ~1300-fold when compared with the natural substrate attached to LovF (Xie et al., 2009a), indicating there is ample opportunity for optimization by protein engineering efforts. Furthermore, the structural basis of LovD function and substrate selection had not been elucidated, limiting our ability to rationally optimize the binding of the unnatural dimethylbutyryl substrate and improve LovD efficiency as a SV synthase.

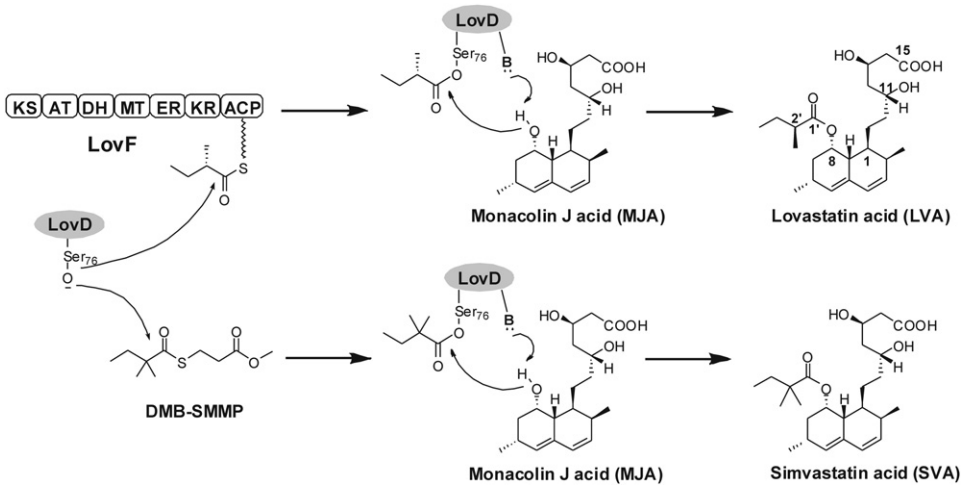

Figure 1. Reactions Catalyzed by LovD

LovD is responsible for converting MJA into LVA via acylation of the α-*S*-methylbutyrate side chain and can also synthesize SVA using DMB-SMMP as an acyl donor.

In this article, we employed directed protein evolution (Arnold and Volkov, 1999) to improve the SV synthase activity of LovD. After seven rounds of screening, LovD mutants with significantly improved catalytic activities and higher thermal stability were isolated. In parallel, seven X-ray crystal structures including the parent LovD G0, an improved mutant G5, and the cocrystal structures of G5 with MJA, LVA, and SVA were obtained. The crystal structures provide atomic-resolution

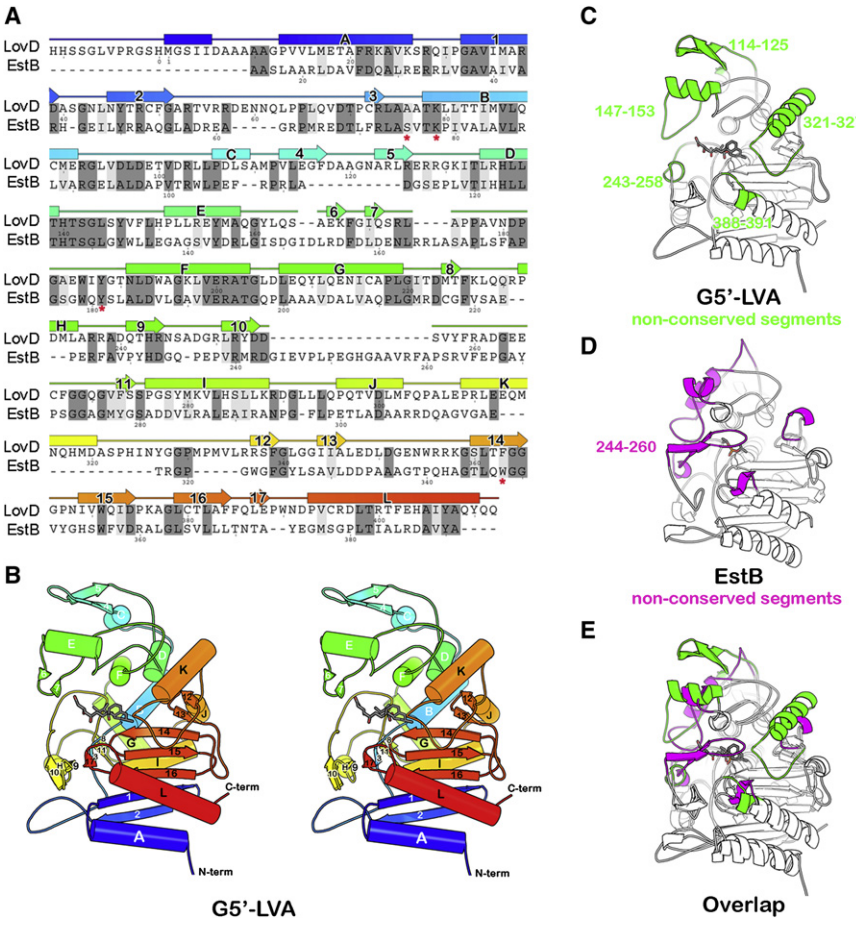

Figure 2. The Crystal Structure of LovD and its Relationship to EstB

(A) A structure-based sequence alignment between LovD and EstB. Secondary structure elements assigned from the structure of LovD are shown above the sequence. The colors are ramped from blue at the N terminus to red at the C terminus. The active site residues in EstB are indicated by an asterisk "*" below the amino acid.

(B) A stereo ribbon diagram showing the G5′-LVA complex.

(C) Structure of LovD. Highlighted in green are segments that are not conserved in EstB. These five loops project around the circumference of the active site like the fingers in a catcher's mitt.

(D) Structure of EstB. Highlighted in magenta are segments that are not conserved in LovD.

(E) The overlay of LovD and EstB structures. Notably absent from LovD is a loop that covers the active site in EstB (residues 244–260).

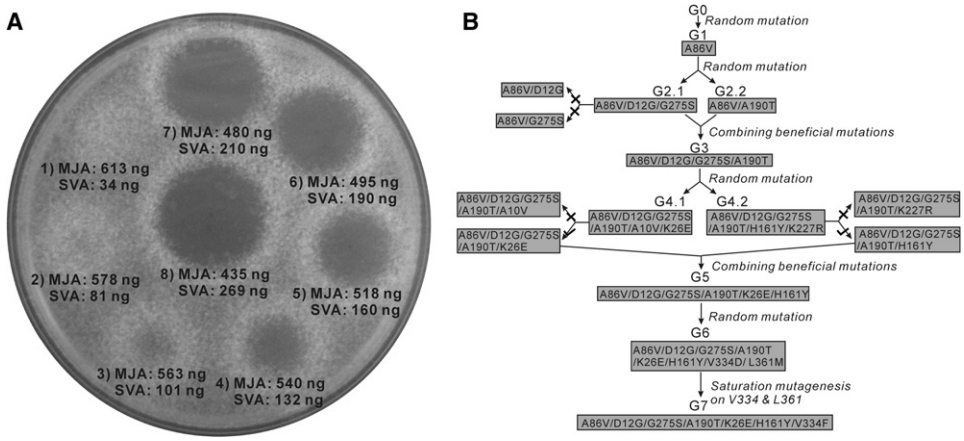

Figure 3. Directed Evolution of LovD as a Simvastatin Synthase

(A) An agar diffusion-based assay was used to quantify the amount of SVA in the whole-cell activity experiments. *N. crassa* was embedded in the agar prior to spotting the reaction mixture. The numbers (1–8) designate different incubation times of 2.5, 4, 5.5, 7, 8, 9, 10, and 12 hr following addition of MJA and DMB-SMMP to *E. coli* expressing wild-type LovD.

(B) Directed evolution of LovD mutants toward higher whole-cell activities. There are a total of seven generations of LovD mutants. Four generations were derived from random mutagenesis including G1, G2.1, G2.2, G4.1, G4.2, and G6. Two generations were derived from combination of beneficial mutations from previous generation mutants including G3 and G5. G7 was derived though saturated mutagenesis of G6 at positions V334 and L361. All mutants with two amino acid changes were subjected to site-directed mutagenesis to determine beneficial or deleterious mutations (G2.1, G4.1, and G4.2). (×) indicates that the mutant had lower whole-cell activity compared with the previous generation. (√) indicates that the mutant had higher whole-cell activity compared with the previous generation.

details regarding the mechanism of catalysis, substrate and product binding, protein-protein interactions with LovF, and a likely explanation for the effects of beneficial mutations on catalysis.

RESULTS

Development of an Agar-Based Diffusion Screening Method

We developed an efficient screening method to assay for *E. coli* expressing LovD mutants with improved properties in the synthesis of SVA from MJA and DMB-SMMP. The assay relied on the growth inhibition of *Neurospora crassa* by statins, a property that was previously exploited in the screening of high LV producing *A. terreus* strains (Kumar et al., 2000). We found that SVA can inhibit the growth of *N. crassa* at submicrogram quantities, whereas inhibition by MJA requires hundred milligram quantities. To demonstrate the sensitivity and feasibility of the assay, an *E. coli* culture expressing wild-type LovD was supplied with 10 mM MJA and 15 mM DMB-SMMP. At different time points, 2 μl aliquots were directly spotted on a Sabouraud's dextrose agar (SDA) plate embedded with *N. crassa* at a density of 0.3∼0.5 × 10^8 spores/l. After 16 hr of incubation at 30°C, different inhibition zones were observed for samples containing different degrees of conversion from MJA to SVA (as verified by high-performance liquid chromatography [HPLC]) (Figure 3A). Based on this screening strategy, any significant contribution to whole-cell LovD activity (defined as the rate of converting MJA to SVA by *E. coli* cultures expressing LovD variants; see Experimental Procedures), such as improvements in solubility, catalytic efficiency and stability, can lead to a detectable phenotypical change.

Screening of LovD Variants with Enhanced Whole-Cell Activities

The starting LovD (generation zero or G0) used in directed evolution is the previously generated double mutant C40A/C60N from wild-type LovD (Xie et al., 2009b). G0 was rationally engineered to be less prone to disulfide-mediated aggregation and was used for crystallization studies (Xie et al., 2009b). The mutant libraries were created by either saturation mutagenesis or error-prone polymerase chain reaction (ep-PCR) that generated an average of 2.5 amino acid changes per round (Fromant et al., 1995). During each round of screening, the mutant library was ligated into pET28(a) and electroplated into YT2 competent cells (Xie et al., 2007). The individual mutants were cultured in 96-well plates, followed by induction of LovD expression, addition of MJA and DMB-SMMP, and spotting onto *N. crassa* embedded plates. Table 1 shows the gradual improvement in whole-cell activity obtained following four rounds of ep-PCR (G1, G2, G4, G6), one round of saturated mutagenesis (G7), and two iterations of combining individual beneficial mutations (G3, G5), with the best mutant G7 displaying ∼11-fold increase in whole-cell activity as a SV synthase compared with G0 (Figure 3B). The mutant G2.1 contains amino acid changes at D12G and G275S. Construction of the corresponding single mutants using G1 as template showed that D12G alone had a large negative effect, whereas G275S alone had a weak positive effect compared with G1. This result suggests the two mutations in G2.1 act synergistically to enhance LovD activities. Combination of mutations from G2.1 and the A190T mutation in G2.2, which was recovered from the same round of ep-PCR, yielded the next-generation mutant G3. Ep-PCR using G3 as a template yielded G4.1 and G4.2, each containing a different double mutation combination of A10V/K26E and H161Y/K227R, respectively.

Table 1. Amino Acid Substitutions and Characterization of LovD Variants

	Mutations	Whole-Cell Activity[a]	k_{cat} (min^{-1})	K_M of MJA (mM)[b]	K_M of DMB-SMMP (mM^{-1})[c]	Soluble Protein (mg/l)[d]	T_m(°C)[e]
G0		1	0.66 ± 0.03	0.77 ± 0.17	0.67 ± 0.12	138 ± 11	39.5 ± 0.4
G1	A86V	1.2	0.79 ± 0.03	0.74 ± 0.16	0.66 ± 0.19	140 ± 5.4	41 ± 0.7
G2.1	A86V D12G G275S	1.9	1.14 ± 0.03	0.91 ± 0.17	0.62 ± 0.10	184 ± 8.7	40.5 ± 0.4
G2.2	A86V A190T	1.8	1.20 ± 0.09	0.74 ± 0.21	0.69 ± 0.17	168 ± 17	41 ± 0.4
G3	A86V D12G A190T G275S	3.6	1.86 ± 0.09	0.77 ± 0.11	0.70 ± 0.19	205 ± 23	41 ± 0.4
G4.1	A86V D12G A190T G275S A10V K26E	4.8	2.13 ± 0.03	0.70 ± 0.24	0.66 ± 0.16	183 ± 18	43.5 ± 0.7
G4.2	A86V D12G A190T G275S H161Y K227R	5.2	2.16 ± 0.12	0.80 ± 0.24	0.64 ± 0.16	221 ± 9.3	42.5 ± 1.9
G5	A86V D12G A190T G275S K26E H161Y	6.4	2.61 ± 0.03	0.74 ± 0.03	0.69 ± 0.14	206 ± 5.7	46.5 ± 0.4
G6	A86V D12G A190T G275S K26E H161Y V334D L361M	9.3	3.30 ± 0.06	0.70 ± 0.07	0.63 ± 0.15	212 ± 3.9	47 ± 0.1
G7	A86V D12G A190T G275S K26E H161Y V334F	11.2	4.80 ± 0.06	0.70 ± 0.04	0.69 ± 0.17	214 ± 6.3	48.5 ± 0.7

[a] The whole-cell activity of LovD mutants are compared with G0, which has a conversion rate of 1.7 mM/hr and is normalized to 1.
[b] K_M of MJA is derived at 25°C when DMB-SMMP is fixed at 2 mM.
[c] K_M of DMB-SMMP is derived when MJA is fixed at 2 mM.
[d] The amounts of soluble proteins are measured from purified protein levels.
[e] Tm is measure by circular dichroism. All results represent mean values of triplicate determinations and standard deviations.

Site-directed mutagenesis confirmed that both A10V and K227R had negative effects on the activities of LovD. Removal of these mutations and combination of K26E and H161Y yielded an improved mutant G5, which was ~6-fold improved in whole-cell activity compared with G0. At this point, structural studies were performed on the G5 mutant to provide insights into the accumulated beneficial mutations. In parallel, an additional round of ep-PCR afforded G6 that contained the beneficial mutations V334D and L361M. Saturation mutagenesis was employed to optimize the combined effects of mutations at positions 334 and 361. The best mutant recovered was G7, of which the whole-cell activity was increased an additional 20%. Surprisingly, we found that while position 334 was altered to phenylalanine, the previously deemed beneficial L361M mutation reverted back to leucine. Site-directed mutation of L361M in G7 confirmed that leucine was indeed the more favorable residue in the context of the V334F mutation.

In Vitro Characterization of LovD Variants

To dissect the contributions that led to the increases in whole-cell activity, kinetic parameters (k_{cat}, K_M), soluble protein levels and thermal stability of all the improved mutants were characterized and listed in Table 1. The binding affinities (K_M) of LovD mutants toward MJA and DMB-SMMP were each within a narrow range (0.7 mM to 0.9 mM for MJA and 0.6 mM to 0.7 mM for DMB-SMMP). The lack of improvement in K_M toward either substrate is not surprising considering the high concentrations of substrates used in the screening assay (~10 K_M of MJA and DMB-SMMP). The observed improvements in whole-cell activity are mainly due to increases in the k_{cat} of the mutants and levels of soluble proteins. The k_{cat} and soluble protein levels were simultaneously increased ~3-fold and ~1.5-fold from G1 to G3, respectively. Impressively, the protein expression levels of G3 reached 205 mg/l. In contrast, improvements in k_{cat} were the sole contribution to the increases in whole-cell activities from round 4 to round 7. Most notably, a single V334F mutation from G5 to G7 nearly doubled the catalytic turnover rate. We also observed a gradual increase in the melting temperature (T_m) of the LovD mutants from 39.5°C to 48.5°C by using circular dichroism. The increases in thermal stability were also reflected in the whole-cell activities of the mutants when expressed at elevated temperatures (see Figure S1 available online). Whereas the G0–G3 mutants have no detectable activity when expressed at 32°C, the later generation mutants retained significant SV synthase activities, with the G7 mutant exhibiting comparable activity to that of G0 at 25°C. Furthermore, the G7 mutant remained active even when expressed at 37°C. The increased thermal stabilities of the mutants have important practical implications in using LovD as a biocatalyst for SV semisynthesis.

To examine the activities of the mutants toward synthesis of the natural biological product LVA, we performed kinetic assays using α-methylbutyryl-SMMP (MB-SMMP) and MJA. A similar trend in the improvements of k_{cat} toward LVA synthesis was observed (Figure S2), indicating the LovD relative substrate specificity toward the acyl group (either MB or DMB) has not changed. Interestingly, when LovF was used in the kinetic assay for LVA synthesis (Figure 1), we observed a progressive loss of activities of the LovD mutants (Figure S2). The G7 mutant exhibited a 27-fold decrease in activities toward LovF compared with the G0 parent, most likely attributed to the deterioration of the required protein-protein interactions for catalysis (Xie et al., 2009a). Therefore, the mutations accumulated during directed evolution might have gradually altered the conformation of LovD to impair its communication with LovF, while not affecting binding of the SMMP-bound acyl group.

Overall Structure of LovD

Seven LovD crystal structures were determined to help illuminate the mechanism of the LovD-catalyzed reaction and possible basis for improved catalysis. These include (1) G0, (2) selenomethionyl G0 (G0-Semet), (3) the improved mutant G5, (4) G5 in complex with substrate MJA, the G5 with S76A active site mutated (called G5′) in complex with (5) LVA, (6) SVA, and (7) MJA. The resolution limits of the structures range from 2.5 to 2.0 Å except for G0. The native G0 structure was resolved at 3.4 Å, but was improved to 2.5 Å in the G0-Semet variant. Refinement statistics are provided in Table 2.

The crystal structure of LovD G0-Semet revealed a variation of the α/β hydrolase fold (Heikinheimo et al., 1999; Nardini and Dijkstra, 1999). It consists of two domains. The first domain (residues 1–92 and 204–413) is a central seven-stranded antiparallel β sheet flanked by α helices on either face (Figures 2B and S3A). A *cis*-peptide bond is formed between Glu388 and Pro389, contributing to a kink in the sheet. The second domain is smaller (residues 93–203) and primarily α-helical. A deep and narrow cleft (11 × 6 Å) is formed at the interface between the two domains. At the bottom of the cleft is the catalytic Ser76 that acts as the nucleophile in the acyltransfer reaction.

Comparison between LovD and EstB

Encircling the active site cleft is a broad, ring-shaped ridge, which is absent from the homologous enzyme EstB. Their structures are superimposable with root-mean-square deviation (rmsd) of only 1.5 Å over 270 pairs of α-carbons (about two-thirds of the structure) (Figure 2E). The similarity is striking for the core of the two enzymes, but they differ notably in the loops peripheral to the active site, both in size and architecture. In LovD, these loops give the impression of a ring-shaped ridge or baseball catcher's mitt over the active site with fingers composed of five loops: residues 114–125, 147–173, 243–258, 321–327, and 388–391 (Figure 2C). The first and last of these loops are longer in LovD than in EstB by 11 and 19 residues, respectively. The second loop is displaced 7 Å from the active site compared with EstB, extending the grasp of the "mitt." Most notably absent from the LovD molecule is the 23-residue loop that if present would obstruct the grasp of the mitt and cover the active site entrance (corresponding to residues 244–260 in EstB) (Figure 2D). The shape and diameter of the ridge surrounding the active site (a circle of 17 Å diameter) satisfies the requirement of accommodating LovD's natural binding partner, the ACP of LovF (Xie et al., 2009a). The distance between the rim of LovD and active site Ser76 is ~20 Å, which is roughly the same as the length of the phosphopantetheine (Ppant) arm of the ACP domain of LovF.

Crystal Structures of the Mutant G5

The LovD G0-Semet structure enables us to identify residues important for catalytic efficiency, which, when mutated to LovD G5, improved the k_{cat} ~4-fold. These residues are scattered widely over space, forming no mutual contacts. Further, because they are located in both buried and solvent exposed regions, they do not share a common physical environment. Moreover, distances of these residues to the active site Ser76 are relatively large, ranging from 10 to 32 Å for Thr190 and Gly12, respectively (Figure 4). The lack of connectivity of the residues to each other and to the active site is a common phenomenon in numerous directed evolution experiments (Hsu et al., 2005; Oue et al., 1999; Zhao and Arnold, 1999).

The crystal structure of G5, however, offered evidence to suggest that the increased activity afforded by its six mutations can be attributed to their ability to stabilize a more closed form of the active site cleft. Comparison of the G0-Semet structure with G5 revealed a rotation about the domain-domain hinge of 5°, narrowing the cleft by about 0.5 Å and producing motions up to 3 Å for atoms furthest from the hinge (Figure 5A). Subsequent structures of G5′ bound to the LVA showed larger movements along the same trajectory arising from a 14° hinge rotation. That observation suggests that the beneficial mutations in the G5 variant help promote a conformational change required for catalysis.

Stabilization of the closed conformation of LovD might enhance activity by positioning residues critical for catalysis. For example, when the large domains of G0-Semet, G5, and G5-MJA are superimposed (residues 14–92 and 204–405), domain rotation from G0-Semet to G5 closes the gap between the guanido group of Arg173 and the C15 carboxylate of MJA by 0.5 Å . This rotation could be attributed to the G5 mutations (and perhaps to a difference in crystal packing) but not to ligand binding, since the comparison is between two unliganded structures. Ligand binding produces a further rotation from G5 to G5-MJA, which closes the gap between Arg173 and MJA by an additional 2.2 Å, so that a hydrogen bond is formed between the two groups. Similarly, G5 mutations bring Phe148 and Tyr188 side chains from the G0-Semet position closer to substrate (G5-MJA), although their motion is smaller because they lie closer to the hinge axis (Figure S4A).

The A86V mutation in particular appears responsible for stabilizing closure of the hinge. Its two additional methyl groups buried in the boundary between domains act as a wedge pushing against Leu134 on the distal side of the hinge axis, thereby closing the active site cleft on the proximal side of the hinge axis (Figure 5A). The beneficial effects of the K26E and G275S mutations are less obvious. The K26E mutation might improve stability of the enzyme by breaking up a patch of positively charged residues (R22, K23, K26, and R28) on the surface of helix A (Figure S5A) (Schweiker et al., 2007). The G275S mutation appears to improve stability of the enzyme by adding a hydrogen bond with the N-terminal end of helix I and decreasing torsional flexibility of the backbone (Figure S5B).

Cocrystallization of LovD G5′ with MJA, LVA, and SVA

Structures of LovD G5′ in complex with substrate and products illustrate the mode of binding of these ligands and suggest a catalytic mechanism for acyl transfer. The substrate MJA binds with its C8-hydroxyl group deep inside the cleft between domains, forming hydrogen bonds with Ser76, Tyr188, and a fortuitously bound formate molecule (used as a cryoprotectant) (Figure 6A). The proximity of the C8-hydroxyl to the Ser76 hydroxyl is consistent with the expectation that both hydroxyl groups initiate a nucleophilic attack on the same acyl group during different steps in the reaction sequence (Figure S6B). The two faces of the decalin ring system of MJA are sandwiched between the aromatic rings of Trp390 and Tyr188 (Figure S3C). Additional hydrophobic and van der Waals interactions with

Table 2. Statistics of X-ray Data Collection and Atomic Refinement

Protein	G0	SeMet G0	G5	G5	G5′	G5′	G5′
Ligand	None	None	None	MJA	MJA	SVA	LVA
Data collection							
Space group	P1	C2	$P2_12_12_1$	$P2_12_12_1$	$P2_12_12_1$	$P2_12_12_1$	$P2_12_12_1$
Cell dimensions							
a, *b*, *c* (Å)	56.7,79.7,104.1	209.5,85.2,104.0	58.2, 75.0, 131.6	58.5, 75.2, 133.5	58.0, 75.2, 132.7	58.5, 75.1, 131.8	59.0, 75.2, 131.7
α, β, γ (°)	94.1,91.6,106.8	90.0,117.5,90.0	90.0, 90.0, 90.0	90.0, 90.0, 90.0	90.0, 90.0, 90.0	90.0, 90.0, 90.0	90.0, 90.0, 90.0
Protomers/ asymmetric unit	4	4	1	1	1	1	1
Resolution (Å)	100.00-3.40	80.00-2.50	90.00-2.00	60.00-2.00	60.00-2.05	60.00-2.00	60.00-2.00
	(3.66-3.40)	(2.59-2.50)	(2.07-2.00)	(2.07-2.00)	(2.12-2.05)	(2.07-2.00)	(2.07-2.00)
R_{merge} (%)	20.8 (43.4)	11.8 (45.3)	4.9 (37.8)	15.6 (39.6)	6.8 (40.2)	6.9 (31.4)	11.8 (39.6)
$I / \sigma I$	5.1 (2.9)	10.2 (1.7)	47.2 (6.5)	13.0 (4.8)	38.3 (6.6)	19.5 (3.9)	13.33(4.64)
Completeness (%)	99.3(98.9)	89.9 (46.7)	99.9 (100.0)	99.8 (100.0)	99.9 (99.8)	97.7 (99.6)	98.5 (99.5)
Redundancy	3.7(3.7)	5.3 (3.0)	11.6 (11.7)	6.2 (6.4)	15.4 (12.9)	4.9(4.9)	6.4(6.5)
Wavelength (Å)	0.9793	0.9793	0.9794	0.9794	0.9792 &1.5418	0.9717	0.9795
Refinement							
Resolution (Å)	103.7- 3.4	65.9- 2.50	65.80- 2.00	46.18- 2.00	49.86- 2.05	49.51- 2.00	46.42- 2.00
	(3.5- 3.4)	(2.56- 2.50)	(2.05- 2.00)	(2.05- 2.00)	(2.10- 2.05)	(2.05- 2.00)	(2.06- 2.00)
No. reflections	22457 (1669)	47728 (1657)	37539 (2837)	38325 (2910)	35223 (2686)	36938 (2714)	37005 (2671)
R_{work} / R_{free} (%)	23.1/27.5 (31.9/35.5)	24.8/29.0 (35.6/40.5)	17.9/20.6 (20.4/24.4)	17.9/21.3 (21.5/26.1)	17.7/20.9 (19.8/23.7)	17.6/20.9 (23.1/25.1)	16.2/18.9 (18.3/21.8)
Number of atoms							
Protein	12328	12547	3289	3332	3355	3351	3343
Ligand/ion 1	0	65 (sulfate)	13 (PEG)	48 (MJA)	24 (MJA)	31(SVA)	30
Ligand/ion 2	0	0	6 (glycerol)	12 (formate)	8 (dithiothreitol)	0	0
Water	0	21	151	275	157	179	230
B-factors (Å^2)							
Protein	6.3	51.7	34.4	27.6	35.4	32.2	31.4
Ligand/ion 1	n/a	68.0 (SO_4)	58.6 (PEG)	58.8 (MJA)	46.5 (MJA)	45.5 (SVA)	38.3 (LVA)
Ligand/ion 2	n/a	n/a	58.2 (glycerol)	38.6 (formate)	74.2 (dithiothreitol)	n/a	n/a
Water	n/a	39.4	36.9	32.8	37.6	36.1	37.2
Rmsds							
Bond lengths (Å)	0.011	0.006	0.009	0.009	0.008	0.008	0.008
Bond angles (°)	1.3	0.995	1.199	1.230	1.202	1.193	1.193
Ramachandran Plot (%)							
Most favored	88.0	90.0	91.2	89.4	89.7	90.3	90.6
Additionally allowed	11.4	9.7	8.5	10.3	10.0	9.4	9.1
Generously allowed	0.6	0.3	0.3	0.3	0.3	0.3	0.3
Disallowed	0.0	0.0	0.0	0.0	0.0	0.0	0.0
PDB ID code	3HL9	3HLB	3HLC	3HLD	3HLE	3HLF	3HLG

$R_{merge} = \Sigma|I - < I >|^2/\Sigma I^2$, where I is the observed intensity. Both summations involve all input reflections for which more than one symmetry equivalent is averaged. $R_{work} = \Sigma||F_o| - |F_c||/\Sigma|F_o|$, where F_o and F_c refer to observed and calculated structure factors, respectively. R_{free} is similar to R_{work}, but is based on a subset of the reflections, which were withheld from refinement for cross validation. Numbers in parentheses refer to the outer shell of data.

the edges of the ring system are observed with Phe363, Ile325, Tyr327, Phe148, Leu149, and the peptide planes of Gly364, Gly365, and Gly366 (Figure S3C). The hydrophilic tail of MJA (i.e., the C1 substituent on the decalin ring) extends away from the active site into bulk solvent. The C11 hydroxyl group hydrogen bonds with the Glu388 side chain and the backbone

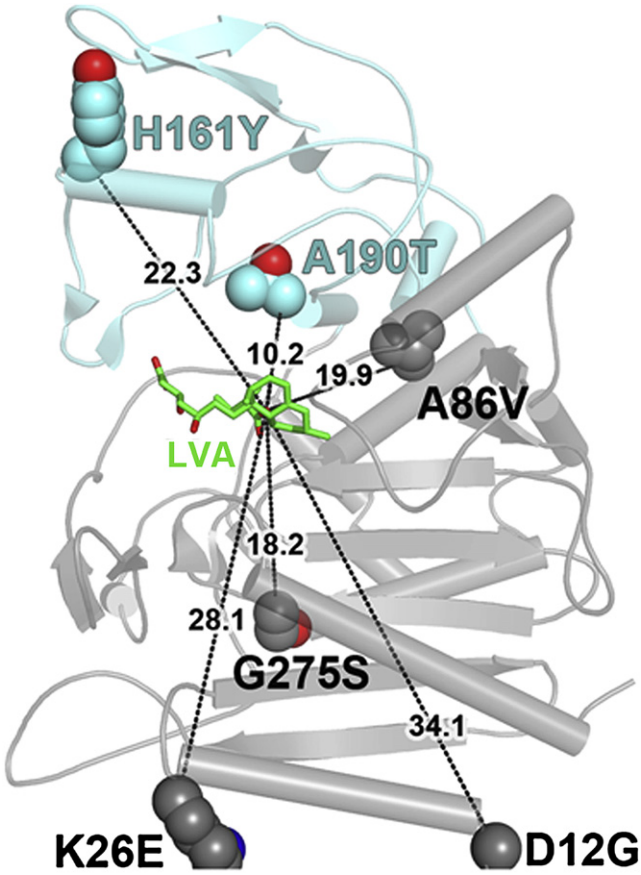

Figure 4. Structure of the G5 Mutant Provides Insight into Improved Catalysis

Positions of the amino acid changes present in the improved mutant G5, highlighting their generally large distances from the active site. Distances are drawn from the amino acid α carbons to the nucleophilic hydroxyl (C8) of LVA (shown in green).

amide of Trp390, the latter being mediated by a water molecule. The C15 carboxylic acid forms a salt bridge with Arg173.

The position of the α-*S*-methylbutyryl group is revealed in the crystal structure of the LovD G5′ mutant in complex with LVA. As in the MJA complex, the decalin ring and hydrophilic tail of LVA bind with similar geometry. Interestingly, the additional methylbutyryl group extends parallel to the MJA hydrophilic tail (Figure 6B). The proximity of the two tails gives LVA a hairpin shape, with the decalin ring forming the hairpin turn between the two tails. The hydrophobic side-chain binding position is likely the site at which the acyl donor binds. The proximity of the tails also suggests how MJA competitively inhibits the acyl transfer reaction when it binds prior to the methylbutyryl substrate (Xie et al., 2006), because the hydrophilic tail of MJA partly obstructs access of the methylbutyryl group to the active site, ordered binding of the substrates is required.

Structural comparisons between complexes of LovD G5′ with LVA and SVA suggest some strain is involved in accommodating the nonnatural product, SVA (Figure 6C). SVA contains an additional methyl group compared with LVA, located on the α-*S*-methylbutyryl moiety. Superimposition using only α carbons in the large domains of the two structures shows nearly identical arrangements of atoms in the large domains and the decalin rings (Figure 6D). But contact between the additional methyl group (attached at C2′) and the side chain of Phe148 appears to push open the cleft between domains. As a result, Phe148 moves approximately 0.8 Å away from its position in the LVA complex (Figure S4B). There is also a 30° rotation about the C1′-C2′ bond of the α-dimethylbutyryl moiety. The consequence of these rotations for the relative catalytic rates of the two substrates appears minor; the movements near the atoms directly involved in acyl transfer are small. This is consistent with the ability of LovD to catalyze acyl transfer using an α-dimethylbutyryl group as substrate instead of the natural α-methylbutyryl group. However, further amino acid mutations, such as the aforementioned Phe148, could improve the fit to the α-dimethylbutyryl substrate, or other variations. The structures presented here provide a framework for such design efforts.

DISCUSSION

In this work, we show that seven amino acid changes led to the ~11-fold increase in the SV synthase activity of LovD. This level of enhancement is significant considering G0 was already an adequate SV synthase following our previous efforts in substrate and strain optimization. Although the kinetic activity of G7 is far below that of the natural reaction catalyzed by LovD using acyl-LovF, G7 is a robust mutant for high-volume synthesis of SVA using the whole-cell platform. When G7 was applied in a high-density fermentation environment, more than 30 g/l MJA was quantitatively converted to SVA within 1 day. The relatively few rounds of direct evolution to achieve the activities of G7 also demonstrate that LovD is highly evolvable as a biocatalyst.

The X-ray crystal structures solved in this work provides insight into different facets of LovD enzymology. Among these, the spatial arrangement of the LovD catalytic triad Ser76-Lys79-Tyr188 was captured and is shown to be consistent with that of the esterase EstB (Figure S6). Tyr188 (as the phenolate) appears to be the general base in initiating the two nucleophilic attacks required for completion of the acyl transfer reaction (Oefner et al., 1990). The first nucleophilic attack is by Ser76 on the α-*S*-methylbutyryl group and the second attack is by the C8 hydroxyl of MJA on the acylated enzyme intermediate. In both reactions, the attacking hydroxyl group must be activated by deprotonation (Figure S6C). Tyr188 is well-positioned to deprotonate both hydroxyl groups, forming hydrogen bonds with Ser76 in the apo-enzyme and with MJA in the G5-MJA complex. Lys79 is also well-positioned to aid in activating the two hydroxyl groups by forming a hydrogen bond relay with Tyr188 in the G5-MJA complex. Site-directed mutation of either Tyr188 or Lys79 to alanine resulted in complete loss of activity.

Details of the α-*S*-methylbutyryl binding pocket suggest how the transition states for the acyl transfer reactions are stabilized. As in the MJA complex, the C8 oxygen of LVA maintains a hydrogen bond to Tyr188, but the neighboring water molecule has been displaced by the carbonyl oxygen of the α-*S*-methylbutyryl group. This carbonyl oxygen forms a pair of hydrogen bonds with the backbone amides of Ala76 (i.e., Ser76 in the G0-Semet) and Gly366. The geometry of the hydrogen bonds appears ideal, with the amide hydrogen atoms pointed directly at the two lone

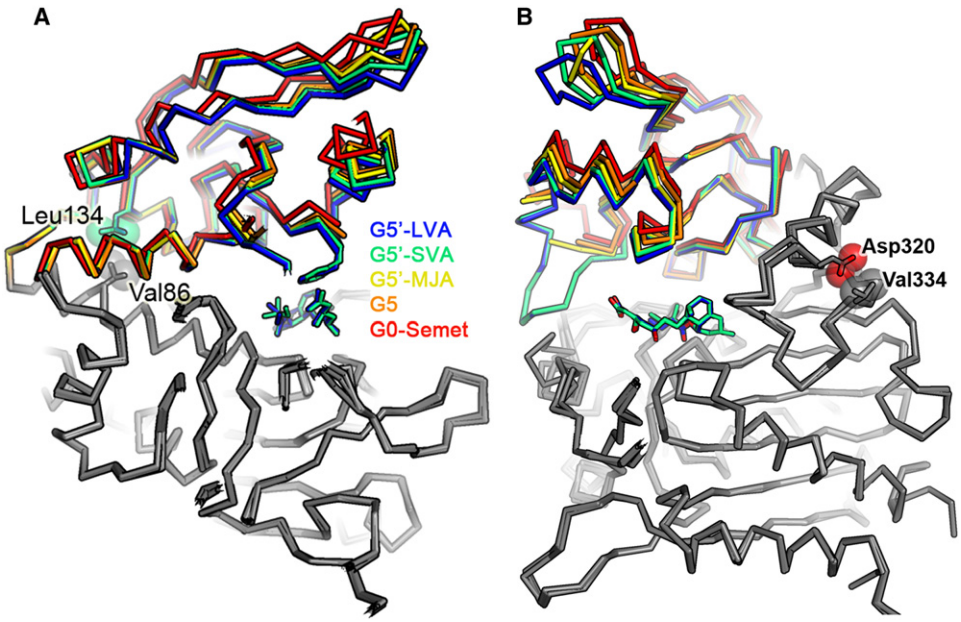

Figure 5. Side View of the Overlap of Five LovD Structures

This representation indicates a hinge rotation between two domains due to G5 mutations and the presence of bound ligands.

(A) Two important residues (Val86 and Leu134), which may stabilize closure of the hinge, are shown in spheres.

(B) Another two residues (Val334 and Asp320) are directly in contact with each other. Mutation V334D in G6 would result in electrostatic repulsion between Asp334 and Asp320, while mutation V334F in G7 could result in steric clash between the phenyl side chain and Asp320. Both could stabilize closure of the hinge.

electron pairs on the carbonyl oxygen. These hydrogen bonds would appear well suited to stabilize a tetrahedral transition state. The closest protein contacts with the aliphatic portion of the methylbutyryl group are aliphatic or aromatic carbons: Ala75 (Cβ), Phe148 (Cζ), Tyr146 (Cζ), and Asn270 (Cβ). Notably, the α-*S*-methylbutyryl aliphatic carbons are also surrounded by three positively charged side chains, Arg73, Lys79, and Arg173, all within 4.1 Å. These positive charges might help stabilize the negative charge of the oxyanion hole that forms during acyl transfer. Indeed, the pocket's affinity for negative charges is demonstrated by the fortuitous presence of a bound formate anion in this position in the G5-MJA complex.

The crystal structures provide plausible explanations for the basis of enhanced catalytic efficiency. Upon ligand binding, LovD undergoes a conformational change analogous to the closing of the catcher's mitt. Movement of the domains shown in Figure 5A positions the catalytic residues in closer proximity to each other and to the ligands, and serves to enhance the rate of catalysis. The G5 structure suggested that beneficial mutations afforded an alternative way to pre-position the active site residues to increase the catalytic efficiency. Although the V334D and V334F mutations of G6 and G7, respectively, were discovered subsequent to the structural work of G5, the molecular explanation above can also be applied to rationalize the beneficial nature of the additional single mutations. Val334 is located in the middle of a loop between helix K and sheet 12. The two side-chain methyl groups of Val334 are directly in contact with the side chain of Asp320 on helix K, which serves as one of the domain-domain hinges and is in contact with the loop where Tyr188 is located (Figure 5B). Mutation of V334 could therefore result in movement of the domains around the helix K hinge. For example, the mutation V334D in G6 would result in electrostatic repulsion between Asp334 and Asp320. Similarly, the mutation V334F in G7 could result in steric clash between the phenyl side chain and the side chain of Asp320, further closing the active site cleft and bringing key residues (e.g., Tyr188) into more optimal positions for catalysis. On the other hand, the more compact conformations of LovD mutants are less compatible with binding to LovF, which apparently favors the open conformation of LovD.

SIGNIFICANCE

SV is the active pharmaceutical ingredient of the blockbuster cholesterol-lowering drug Zocor®. Semisynthesis of SV from LV is therefore an intensely pursued target for devising an efficient biocatalytic approach. Our previously developed platform for the biosynthesis of SV was powerful, but still suboptimal due to the lack of a robust biocatalyst. In this work, we employed directed evolution to engineer LovD. Several better mutants were obtained and the best mutant "G7" displayed an ~11-fold increase in whole-cell biosynthesis of SVA compared with the parent G0. Catalytic efficiency, solubility, and thermostability were improved simultaneously. We have determined seven X-ray crystal structures including the parent LovD G0, an improved mutant G5, and the cocrystal structures of G5′ with MJA, LVA, and SVA. The structure information not only aided our understanding of the catalytic mechanism of LovD, but also afforded insights into how mutations affected the overall properties of LovD. Comparing the structures between LovD G0 and G5 suggests the beneficial mutations help

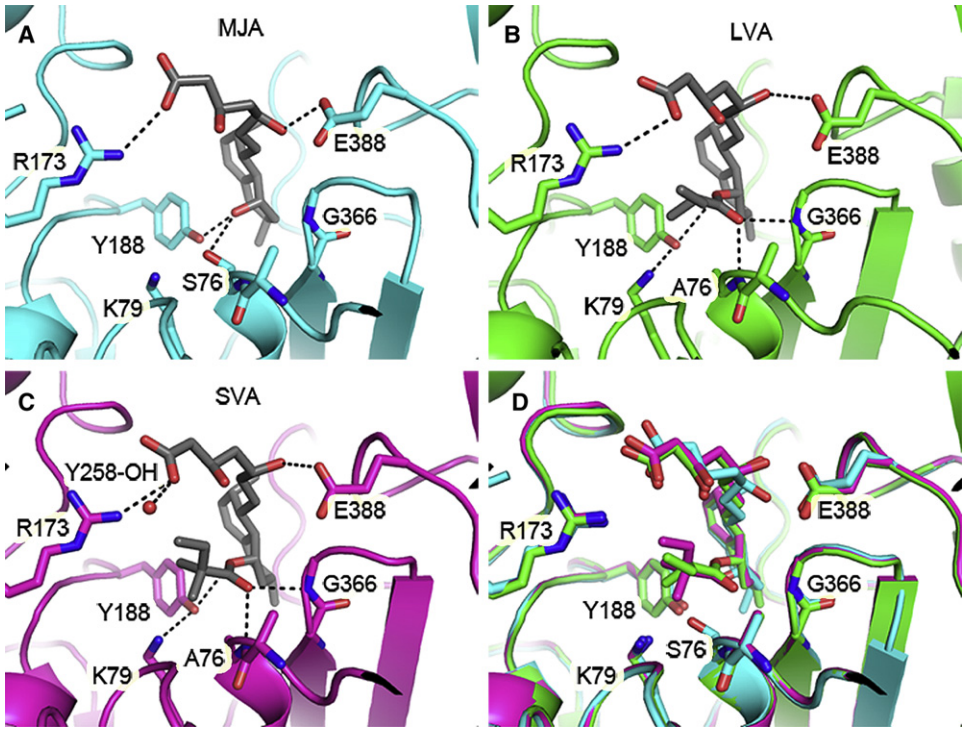

Figure 6. Comparison of the LovD Active Site Bound with Different Ligands

(A) G5 in complex with substrate MJA.

(B) G5′ in complex with product LVA.

(C) G5′ in complex with product SVA.

(D) Overlay of the three structures showing conformational changes, particularly at the nucleophilic serine, associated with binding to different ligands. Dashed lines represent hydrogen bonds. The active site entrance is at the top of each figure. Some residues involved in ligand binding are not shown.

promote a more compact conformation required for catalysis. The cocrystallization of LovD G5′ with substrate MJA, product LVA and SVA reveals how acyl transfer reaction proceeds via a ping-pong mechanism, how MJA becomes a competitive inhibitor, and how the catalytic cavity is adapted to accommodate its nonnatural product. Our work, therefore, can have significant impact on biocatalyst development and provides insights into fundamental understanding of enzymology.

EXPERIMENTAL PROCEDURES

Ep-PCR and Construction of Mutant Library

Ep-PCR procedure was modified from established protocols (Fromant et al., 1995). The reaction consisted of 0.35 mM dATP, 0.4 mM dCTP, 0.2 mM dGTP, 1.35 mM dTTP, 4 mM $MgCl_2$, 0.25 mM $MnCl_2$, and 2.5 U Taq polymerase. The reaction mixture was submitted to 25 cycles of PCR: 94°C for 1 min, 55°C for 1 min, and 72°C for 3 min. The resulting PCR products were digested with DpnI, further digested with EcoRI and NdeI, and ligated to pET28(a). The ligation mixture was transformed to YT2 and plated on LB agar containing 35 mg/l kanamycin.

Selection of High Activity Mutants

N. crassa was grown on SDA slants for 10 days and spores were harvested with 1% Tween-80. Then 100 ml molten SDA was seeded with 0.3–0.5 × 10^8 spores and poured into a 230 × 230 mm plate. Colonies from mutation library were cultured in 96 well plates containing 250 μl LB medium (with 35 mg/l kanamycin). The cells were grown at 37°C to saturation and transferred to duplicated plates. Protein expression was induced with 0.1 mM IPTG at OD_{600} of 0.5 and the expression was performed at 25°C for 16 hr. Then 5 mM MJA and 10 mM DMB-SMMP were added to initiate the reaction. After a certain reaction time (45 min to 4 hr depending on the activity of the parent), cells were removed with centrifugation (2000 g, 4°C, 5 min). The amount of supernatant spotted on the SDA plate was typically 1∼3 μl. The plates were incubated at 30°C for 16∼18 hr. The improved mutants were selected following visual comparison of the inhibition zones. Normally, one or two improved mutants can be obtained from screening ∼2000 mutants in 2 weeks.

Site-Directed Mutagenesis

Site-directed mutations were performed using the standard QuikChange strategy using relevant templates. The primers were ordered from IDT (Integrated DNA Technologies). All mutations were verified by DNA sequencing (Laragen, Los Angeles, CA).

Saturation Mutagenesis

The LovD G6 gene was randomly mutated at positions of V334 and L361. Because the two residues are close to each other, the two random mutations were introduced in a single pair of primers. Two segments were amplified by PCR and linked together using slice-by-overlap extension (SOE) PCR to give intact LovD gene, which was subsequently introduced to pET28(a).

Determining Whole-Cell Biocatalysis Activity

Parent LovD G0 and all mutants were cultured in parallel for comparison. A single colony of the freshly transformed YT2 competent cells was used to inoculate a 5 ml LB culture supplemented with 35 mg/l kanamycin. Following overnight growth at 37°C, 100 μl culture was inoculated into 50 ml LB medium

supplemented with 35 mg/l kanamycin. When OD_{600} reached 0.4∼0.6, 0.1 mM IPTG was added to the cultures and expression of all LovD variants was performed at 25°C for 16 hr. To mimic the high density fermentation conditions, the cells were then concentrated 10-fold before addition of substrates. A 10 ml aliquot of each culture was collected by centrifugation (4°C, 2000 g, 10 min). The cell pellet was gently resuspended in 1 ml medium supernatant, followed by addition of 70 μl MJA (300 mM stock) to a final concentration of 15 mM. The concentrated culture was then divided into seven 200 μl aliquots and 1 μl pure DMB-SMMP was added to each sample to a final concentration of 20 mM. The small cultures were then shaken at 300 rpm at 25°C. At each time point, a complete extraction of one culture aliquot was performed by adding 10 μl 20% SDS for cells lysis, followed by extraction with 500 μl ethyl acetate containing 1% trifluoroacetic acid (TFA). The organic phase was removed, evaporated, and redissolved in 500 μl acetonitrile for HPLC analysis. The whole-cell activity was determined by fitting the linear regions of the conversion time course plot.

Kinetic Assay of LovD Variants toward MJA and DMB-SMMP

To obtain K_M values for MJA and k_{cat}, the DMB-SMMP concentration was fixed at 2 mM, while the concentration of MJA was varied from 0.25 to 5 mM. To obtain K_M values for DMB-SMMP and k_{cat}, the MJA concentration was fixed at 2 mM, while the concentration of DMB-SMMP was varied from 0.5 to 5 mM. Dimethyl sulfoxide (DMSO) was added to a final concentration of 10% to facilitate the solubilization of DMB-SMMP. At different time points of the kinetic assay, an aliquot of the reaction mixture was removed, quenched with 1% TFA, and extracted with EA containing 1% acetic acid. The organic phase was separated, dried, resolubilized by acetonitrile (ACN), and analyzed by a Beckman Gold HPLC using a reverse-phase C18 column (Alltech Apollo 5i, 150 mm × 4.6 mm) and a linear gradient: 60% ACN in water (0.1% TFA) to 95% ACN in water (0.1% TFA) for 10 min, 1 ml/min. Conversion of MJA to SVA was measured by integration of the peaks at 238 nm.

Kinetic Assay of LovD Variants toward MB-SMMP

To compare the k_{cat} of LovD mutants toward lovastatin synthesis using MB-SMMP as the substrate, both MJA and MB-SMMP were fixed at 2 mM. DMSO was added to a final concentration of 10% to facilitate the solubilization of MB-SMMP. At different time points of the kinetic assay, an aliquot of the reaction mixture was removed, quenched with 1% TFA, and extracted with EA containing 1% acetic acid. The organic phase was separated, dried, resolubilized by ACN, and analyzed HPLC using the same program described above.

In Vitro Assay of LovD Variants toward LovF

Fifty micromoles of LovF (Xie et al., 2009a) was incubated with 1 μM LovD variants, 2 mM MJA, 2 mM malonyl-CoA, 2 mM S-(5′-adenosyl)-L-methionine chloride (SAM), 2 mM NADPH in 100 mM phosphate-buffered saline (pH 7.4). At 1 hr and 2 hr time points, an aliquot of the reaction mixture was removed, quenched with 1% TFA, and extracted with EA containing 1% acetic acid. The organic phase was separated, dried, resolubilized by ACN, and analyzed by HPLC using the same program described above.

Comparing Expression Levels of Soluble LovD

Each expression plasmid encoding *LovD* mutant was transformed into *E. coli* BL21(DE3). The transformant was cultured in 50 ml LB medium containing 35 mg/l kanamycin at 37°C to optical density (OD_{600}) value of 0.4∼0.6. Protein expression was induced with 0.1 mM IPTG and the subsequent expression was performed at 25°C for 16 hr. Cells were collected by centrifugation (2000 g, 4°C, 15 min), resuspended in 7 ml Buffer A (50 mM Tris–HCl [pH 8.0], 2 mM DTT, 2 mM EDTA), and lysed by sonication. Cell debris and insoluble proteins were removed by centrifugation (20,000 g, 4°C, 1 hr). To the cleared cell lysate, excess amount (0.5 ml) of Ni-NTA resin (QIAGEN, Valencia, CA) was added to each sample. The mutants were then purified using a step gradient of Buffer A with increasing concentration of imidazole (10, 20, and 250 mM). LovD variants were eluted with 5 ml Buffer A containing 250 mM imidazole. No LovD protein was found in other fractions. The protein concentrations were qualitatively assessed by SDS-PAGE and quantitatively determined by the Bradford protein assay using bovine serum albumin as the standard.

T_m Measurement by Circular Dichroism

Samples were prepared by adding 50 μg proteins to 250 μl 10 mM Tris-HCl buffer (pH 7.0). The sample was placed in a quartz cuvette with a 1 cm path length and heated in a Peltier-controlled cell at a rate of 1°C per min. Ellipticity was monitored at 222 nm in a Jasco spectropolarimeter (Jasco Inc., Easton, MD). The midpoint of the denaturation curve was determined with Microcal Origin 5.0 software (OriginLab Corporation, Northampton, MA).

ACCESSION NUMBERS

The coordinates and structure factors for G0, SeMet G0, G5, G5-MJA, G5′-MJA, G5′-LVA, and G5′-SVA have been deposited in the Protein Data Bank under ID codes 3HL9, 3HLB, 3HLC, 3HLD, 3HLE, 3HLF, and 3HLG, respectively.

SUPPLEMENTAL DATA

Supplemental data include six figures and Supplemental Experimental Procedures and can be found with this article online at http://www.cell.com/chemistry-biology/supplemental/S1074-5521(09)00327-5.

ACKNOWLEDGMENTS

This work was supported by American Heart Association (0535069N, to Y.T.) and the National Institutes of Health (1R21HL091197, to Y.T. and T.O.Y.). The authors thank Duilio Cascio and the staff of the Advance Photon Source beamline 24-ID-C for assistance with data collection.

Received: September 12, 2009
Revised: September 24, 2009
Accepted: September 28, 2009
Published: October 30, 2009

REFERENCES

Arnold, F.H. (2001). Combinatorial and computational challenges for biocatalyst design. Nature *409*, 253–257.

Arnold, F.H., and Volkov, A.A. (1999). Directed evolution of biocatalysts. Curr. Opin. Chem. Biol. *3*, 54–59.

Berg, V.A., Hans, M., and Steekstra, H. (2009). Method for the production of simvastatin. WO2007147801 (A1).

Fromant, M., Blanquet, S., and Plateau, P. (1995). Direct random mutagenesis of gene-sized DNA fragments using polymerase chain-reaction. Anal. Biochem. *224*, 347–353.

Heikinheimo, P., Goldman, A., Jeffries, C., and Ollis, D.L. (1999). Of barn owls and bankers: a lush variety of alpha/beta hydrolases. Structure *7*, R141–R146.

Hoffman, W.F., Alberts, A.W., Anderson, P.S., Chen, J.S., Smith, R.L., and Willard, A.K. (1986). 3-Hydroxy-3-methylglutaryl-coenzyme A reductase inhibitors. 4. side-chain ester derivatives of mevinolin. J. Med. Chem. *29*, 849–852.

Hsu, C.C., Hong, Z.Y., Wada, M., Franke, D., and Wong, C.H. (2005). Directed evolution of D-sialic acid aldolase to L-3-deoxy-manno-2-octulosonic acid (L-KDO) aldolase. Proc. Natl. Acad. Sci. USA *102*, 9122–9126.

Istvan, E.S., and Deisenhofer, J. (2001). Structural mechanism for statin inhibition of HMG-CoA reductase. Science *292*, 1160–1164.

Kennedy, J., Auclair, K., Kendrew, S.G., Park, C., Vederas, J.C., and Hutchinson, C.R. (1999). Modulation of polyketide synthase activity by accessory proteins during lovastatin biosynthesis. Science *284*, 1368–1372.

Kumar, M.S., Kumar, P.M., Sarnaik, H.M., and Sadhukhan, A.K. (2000). A rapid technique for screening of lovastatin-producing strains of Aspergillus terreus by agar plug and Neurospora crassa bioassay. J. Microbiol. Methods *40*, 99–104.

Loncaric, C., Merriweather, E., and Walker, K.D. (2006). Profiling a taxol pathway 10 beta-acetyltransferase: Assessment of the specificity and the

production of baccatin III by in vivo acetylation in *E. coli*. Chem. Biol. *13*, 309–317.

Morgan, B., Burk, M., Levin, M., Zhu, Z., Chaplin, J., Kustedjo, K., Huang, Z., and Greenberg, W. (2006). Methods for making simvastatin and intermediates. WO2005040107 (A2).

Nardini, M., and Dijkstra, B.W. (1999). Alpha/beta hydrolase fold enzymes: the family keeps growing. Curr. Opin. Struct. Biol. *9*, 732–737.

Neumann, C.S., Fujimori, D.G., and Walsh, C.T. (2008). Halogenation strategies in natural product biosynthesis. Chem. Biol. *15*, 99–109.

Oefner, C., Darcy, A., Daly, J.J., Gubernator, K., Charnas, R.L., Heinze, I., Hubschwerlen, C., and Winkler, F.K. (1990). Refined crystal-structure of beta-lactamase from citrobacter-freundii Indicates a mechanism for beta-lactam hydrolysis. Nature *343*, 284–288.

Oue, S., Okamoto, A., Yano, T., and Kagamiyama, H. (1999). Redesigning the substrate specificity of an enzyme by cumulative effects of the mutations of non-active site residues. J. Biol. Chem. *274*, 2344–2349.

Petersen, E.I., Valinger, G., Solkner, B., Stubenrauch, G., and Schwab, H. (2001). A novel esterase from Burkholderia gladioli which shows high deacetylation activity on cephalosporins is related to beta-lactamases and DD-peptidases. J. Biotechnol. *89*, 11–25.

Rix, U., Fischer, C., Remsing, L.L., and Rohr, J. (2002). Modification of post-PKS tailoring steps through combinatorial biosynthesis. Nat. Prod. Rep. *19*, 542–580.

Schweiker, K.L., Zarrine-Afsar, A., Davidson, A.R., and Makhatadze, G.I. (2007). Computational design of the Fyn SH3 domain with increased stability through optimization of surface charge charge interactions. Protein Sci. *16*, 2694–2702.

Wagner, U.G., Petersen, E.I., Schwab, H., and Kratky, C. (2002). EstB from Burkholderia gladioli: a novel esterase with a beta-lactamase fold reveals steric factors to discriminate between esterolytic and beta-lactam cleaving activity. Protein Sci. *11*, 467–478.

Xie, X., and Tang, Y. (2007). Efficient synthesis of simvastatin by use of whole-cell biocatalysis. Appl. Environ. Microbiol. *73*, 2054–2060.

Xie, X., Watanabe, K., Wojcicki, W.A., Wang, C.C., and Tang, Y. (2006). Biosynthesis of lovastatin analogs with a broadly specific acyltransferase. Chem. Biol. *13*, 1161–1169.

Xie, X., Wong, W.W., and Tang, Y. (2007). Improving simvastatin bioconversion in Escherichia coli by deletion of bioH. Metab. Eng. *9*, 379–386.

Xie, X., Meehan, M.J., Xu, W., Dorrecstein, P.C., and Tang, Y. (2009a). acyltransferase mediated polyketide release from a fungal megasynthase. J. Am. Chem. Soc. *131*, 8388–8389.

Xie, X., Pashkov, I., Gao, X., Guerrero, J.L., Yeates, T.O., and Tang, Y. (2009b). Rational improvement of simvastatin synthase solubility in Escherichia coli leads to higher whole-cell biocatalytic activity. Biotechnol. Bioeng. *102*, 20–28.

Zhang, C., Griffith, B.R., Fu, Q., Albermann, C., Fu, X., Lee, I.K., Li, L.J., and Thorson, J.S. (2006). Exploiting the reversibility of natural product glycosyltransferase-catalyzed reactions. Science *313*, 1291–1294.

Zhao, H., and Arnold, F.H. (1999). Directed evolution converts subtilisin E into a functional equivalent of thermitase. Protein Eng. *12*, 47–53.

Zhou, H., Xie, X., and Tang, Y. (2008). Engineering natural products using combinatorial biosynthesis and biocatalysis. Curr. Opin. Biotechnol. *19*, 590–596.

